Connexin37 Forms High Conductance Gap Junction Channels with Subconductance State Activity and Selective Dye and Ionic Permeabilities

Richard D. Veenstra,* Hong-Zhan Wang,* Eric C. Beyer,‡ S. V. Ramanan,§ and Peter R. Brink§*

Department of Pharmacology, SUNY Health Science Center at Syracuse, Syracuse, New York 13210; ‡Departments of Pediatrics and Cell Biology and Physiology, Washington University School of Medicine, St. Louis, Missouri 63110; and §Department of Physiology and Biophysics, SUNY Health Science Center at Stony Brook, Stony Brook, New York 11794 USA

ABSTRACT Gap junctions are thought to mediate the direct intercellular coupling of adjacent cells by the open-closed gating of an aqueous pore permeable to ions and molecules of up to 1 kDa or 10–14 Å in diameter. We symmetrically altered the ionic composition or asymmetrically added 6-carboxyfluorescein (6-CF, M_r = 376), a fluorescent tracer, to pairs of connexin37-transfected mouse neuro2A cells to examine the ionic and dye permeability of human connexin37 channels. We demonstrate that the 300-pS channel formed by connexin37 has an effective relative anion/cation permeability ratio of 0.43, directly converts to at least one intermediate (63 pS) subconductance state, and that 6-CF dye transfer is accompanied by a 24% decrease in unitary channel conductance. These observations favor a new interpretation of the gap junction pore consistent with direct ion-channel interactions or electrostatic charge effects common to more conventional multistate ion channels. These results have distinct implications about the different forms of intercellular signaling (cationic, ionic, and/or biochemical) that can occur depending on the expression and conformation of the connexin channel proteins.

INTRODUCTION

Gap junction channels allow the cytoplasmic exchange of ions and small molecules (e.g., cAMP, IP_3, Ca^{2+}) between adjacent cells (Tsien and Weingart, 1976; Dunlap et al., 1987; Saez et al., 1989). From permeable tracer studies, the channel is believed to be an aqueous pore 1.0 to 1.5 nm in diameter with a slight negative charge that permits the passage of soluble molecules of up to 1000 Da in size between mammalian cells (Flagg-Newton et al., 1979; Brink and Dewey, 1980; Schwarzmann et al., 1981; Makowski et al., 1984; Verselis and Brink; 1986; Imanaga et al., 1987). According to the simple pore model, the maximal conductance of an ion channel is limited by the physical dimensions (length and cross sectional area) of the pore and resistivity of the electrolyte solution (Hille, 1992). There is general agreement between the estimated channel conductance of 100 pS (Simpson et al., 1977) and experimentally determined channel conductances of several vertebrate gap junction channels (Neyton and Trautmann, 1985; Veenstra and DeHaan, 1986; Spray and Burt, 1990).

Gap junction channels are formed by different subunit proteins (connexins, Cx) that share a common membrane topology (Beyer et al., 1990). Primary amino acid sequence analysis indicates that the four transmembrane and two extracellular loop domains are highly conserved in all members of the connexin family of gap junction proteins. The connexin-specific sequences are located in the cytoplasmic domains of each protein and may provide unique physiological regulatory and channel properties to the gap junctions in the tissues where these various connexins are expressed. Gap junctions derived from the functional expression of cloned connexin DNAs in *Xenopus* oocytes or communication-deficient mammalian cell lines exhibit distinct transjunctional voltage sensitivities and unitary channel conductances (Swenson et al., 1989; Werner et al., 1989; Fishman et al., 1991; Moreno et al., 1991b; Veenstra et al., 1992). Under similar ionic conditions, connexin-specific channels have maximal unitary conductances ranging from 30 to 240 pS (Veenstra et al., 1992; Reed et al., 1993; Rup et al., 1993; Fishman et al., 1991; Moreno et al., 1991a). Given the disparate channel conductances formed by the distinct connexins, we predict that the molecular permeability of gap junctions will vary depending on the type of connexin expressed. Dye or ion permeability studies of gap junctions in native tissues are complicated by the expression of multiple connexins in a given tissue such as liver or heart (Nicholson et al., 1987; Kanter et al., 1992). Hence, the apparent permeability properties of native gap junctions are likely to be determined by the collective permeability characteristics of the highly expressed endogenous connexins. Therefore, the functional connexin expression by stable transfection has a distinct advantage over native gap junctions for detailed studies of the permeability properties of connexin-specific gap junction channels.

Connexin37 (Cx37) forms a maximum 219 ± 22 pS channel when transfected into N2A cells (Reed et al., 1993). The macroscopic junctional conductance (g_j) of Cx37 gap junctions is sensitive to transjunctional voltages (V_j), having a half-inactivation voltage (V_0) of ±28 mV and a minimum

Received for publication 14 January 1994 and in final form 23 March 1994.

Address reprint requests to Richard D. Veenstra, Department of Pharmacology, SUNY Health Science Center, 750 East Adams Street, Syracuse, NY 13210. Tel.: 315-464-7997; Fax: 315-464-8000; E-mail: veenstrr@vax.cs.hscsyr.edu.

0006-3495/94/06/1915/14 $2.00

normalized steady-state junctional conductance (G_{min}) of 0.27. Assuming that junctional conductance is proportional to the open probability of the channels, these results suggest that the Cx37 channels are most likely to be open when $V_j \leq \pm 30$ mV. The physiological relevance of different channel conductances formed by the connexin family of proteins has yet to be examined. According to the simple pore model, higher channel conductances (γ_j) should be directly correlated with increasing diameter aqueous pores. This translates into an ionic selectivity that should closely resemble the aqueous mobilities of the permeant ions (Eisenman sequence 1; Eisenman, 1962) and an increasing upper size permeability limit for hydrophilic molecules.

In this report, we examine the relative conductances of gap junction channels formed by Cx37, expressed by stable cDNA transfection in communication-deficient mouse neuro2A (N2A) cells (Reed et al., 1993), in the presence of the fluorescent dye (6-carboxyfluorescein, 6-CF) and differing symmetrical ionic (Kglutamate/KCl) conditions. The N2A cell line was chosen for stable connexin cDNA transfection because connexin RNA expression was not detectable in Northern blots with cDNA probes for 11 known connexins (Cx26, Cx31, Cx32, Cx37, Cx40, Cx42, Cx43, Cx45, Cx46, Cx50, and Cx56; Veenstra et al., 1992). Additionally, the presence of multiple conductance states in some tissues has led to speculation that gap junction channels exhibit subconductance states of the fully open channel main state (Chen and DeHaan, 1992). Our results provide the first definitive evidence for the presence of subconducting states of connexin-specific gap junction channels and suggest that the formation of multiple conductance intercellular channels conveys distinct connexin- and conductance state-specific ionic and dye permeability properties on the gap junctions in the tissues where they are expressed.

MATERIALS AND METHODS

Cell culture and transfection

Mouse N2A neuroblastoma cells (ATCC CCL131) were obtained from the American Type Culture Collection (Rockville, MD). N2A cells were grown in minimal essential medium (GIBCO/BRL, Gaithersburg, MD) supplemented with 10% heat-inactivated (56°C for 30 min) fetal calf serum (JRH Biosciences, Lenexa, KS), 1x nonessential amino acids, 2 mM L-glutamine, 100 units/ml penicillin, and 100 units/ml streptomycin (GIBCO/BRL).

The full length cDNA for human Cx37 was cloned into the *Eco*RI site of the eukaryotic expression vector pSFFV-neo (Fuhlbridge et al., 1988). N2A cells in 60-mm dishes were transfected with 20 μg of linearized plasmid using the lipofectin reagent (GIBCO/BRL) according to manufacturer's directions, and stable neomycin-resistant colonies were selected in 0.5 mg/ml G418 (GIBCO/BRL). Connexin expression was verified by Northern blotting of total RNA prepared from selected clones (Veenstra et al., 1992; Reed et al., 1993).

Electrophysiological recordings and solutions

Connexin-transfected N2A cell cultures were plated at low density (2×10^5 cells/35-mm dish) for 12–24 h, washed with HEPES-buffered saline (in mM: 142 NaCl, 1.3 KCl, 0.8 $MgSO_4$, 0.9 NaH_2PO_4, 1.8 $CaCl_2$, 5.5 dextrose, and 10 HEPES, pH 7.2) and examined on the stage of an inverted phase-contrast light microscope (Olympus IMT-2). Cx37-induced coupling in the transfected N2A cells was studied by double whole cell recording (DWCR) procedures as described previously (Veenstra and Brink, 1992). Patch electrodes had resistances of 2–5 MΩ when filled with one of four internal pipette solutions. The composition of the internal pipette solutions are listed in Table 1. When pipette solutions containing CsCl and TEACl were used, 15 mM CsCl and 10 mM TEACl were also added to the HEPES-buffered saline solution. All experiments were performed at room temperature (20–22°C).

Transjunctional potentials (V_j) were elicited by stepping the holding potential of the prejunctional cell (V_1) from a common holding potential ($V_1 = V_2 = 0$ mV, where V_2 is the holding potential of the postjunctional cell) to a new value (V_1') for a minimum of 10 s. $V_j = V_1' - V_2$ when the input resistances of cell 1 and cell 2 are 100-fold higher (e.g., 2 GΩ) than the resistances of the respective whole cell patch electrodes (e.g., 20 MΩ). Junctional current signals appear as simultaneous events of equal amplitude and opposite polarity and the true junctional current (I_j) = $-\Delta I_2(1 + R_{el}/R_{in})$, where ΔI_2 = difference in holding current of cell 2, R_{el} = patch electrode series resistance, and R_{in} = cellular input resistance. When R_{in2} and the junctional resistance are >2 GΩ and are 100-fold higher than the resistance of the recording electrode ($R_{el2}/R_{in2} < 0.01$), $-I_j \approx \Delta I_2$ (<2% error) and the ΔI_2 signal is used to measure the junctional channel current amplitudes. Junctional conductance or resistance was determined from the expression $g_j = 1/R_j = I_j/V_j$, provided that the above conditions are met (Veenstra and Brink, 1992). All current and voltage records were stored on VCR tape using a 4-channel digitizing unit (DR-484 Neuro-corder, Neuro Data Instruments Corp, New York, NY) and VCR tape recorder (Sansui SV-7700) for off-line analysis.

Channel current analysis

For simplicity, junctional channel currents were displayed as paired whole cell currents and all-points current amplitude histograms were compiled from the ΔI_2 trace for each experiment. When recording single gap junction channel currents from a cell pair with $g_j < 0.5$ nS, all of the above conditions are met and $-I_j \approx \Delta I_2$. All analog signals were low pass filtered (8-pole Bessel, LPF-30, WPI, Inc., Sarasota, FL) at 100 Hz and digitized at 2 kHz using a DT2801A A/D board (Data Translation, Inc. Marlboro, MA) installed in an IBM PC/AT clone (Everex 386SX/20). The dead time of the recording instrumentation was 1.8 ms.

The Gaussian distributions present in the all-points current amplitude histograms were fitted with a probability density function of the form

$$f_1(M) = \sum_{n=0}^{M} B(M, n, p_1) f_b(I - I_n, \sigma_b^2 + n\sigma_o^2),$$

where M = number of channels in the junction, n = number of simultaneously

TABLE 1 Composition of internal pipette solutions

Component	IPS #1	IPS #2	IPS #3
mM			
K glutamate	110	120	—
KCl	—	—	120
CsCl	—	15	15
TEACl	—	10	10
NaCl	15	—	—
KH_2PO_4	1	1	1
$MgCl_2 \cdot 6H_2O$	4.6	3	3
$CaCl_2 \cdot 2H_2O$	0.068	0.068	0.068
EGTA	5	5	5
HEPES	25	25	25
Na_2ATP	3	3	3
Na_2CP	3	3	3
Osmolarity (mOsm)	274	311	316
pH	7.0	7.0	7.0

open channels, p_1 = channel open probability, σ_b^2 = variance of the baseline noise, σ_o^2 = variance of the open channel noise, and I_n = current of n open channels (Manivannan et al., 1992). The binomial distribution

$$B(M, n, p_1) = \frac{M!}{n!\,(M-n)!} p_1^n (1-p_1)^{M-n}$$

assumes that there are M independent and identical channels, each channel having an open probability of p_1 (Colquhoun and Hawkes, 1983). Because the area under each peak in an all-points amplitude histogram is equal to the cumulative open time of every nth channel state, fitting the relative amplitudes of the peaks provides a direct estimate of the product of $M \times p_o$ for the observed channel activity. The Gaussian distribution

$$f_b(I - I_n, \sigma_b^2 + n\sigma_o^2) = \frac{1}{\sigma_b\sqrt{2\pi}} \times e^{-(I-I_n)^2/2(\sigma_b^2 + n\sigma_o^2)}$$

defines the mean current amplitude and variance of each peak in the histogram. When the amplitude histogram cannot be fitted by the above functions, the additional assumption is made that of N total channels in the junction, $N - M$ have the property stated above, while the remaining M channels have a different open probability, p_2. The solution to this set of conditions is

$$f_1(N) = \sum_{n=0}^{N}\left[\sum_{k=0}^{n} B(N-M, k, p_1)B(M, n-k, p_2)\right] \times f_b(I - I_n, \sigma_b^2 + n\sigma_o^2)$$

(Manivannan et al., 1992). Similar sets of equations can be derived, assuming that the second population of channels has a different open current amplitude and open variance. Hence, accurate fits of the current amplitude histogram can be obtained when N channels are not independent and identical.

In certain instances, the amplitude histograms cannot be described accurately using the above expressions for independent channels because of the existence of intermediate conductance states. Alternative expressions assuming the existence of long-lived channel substates have been derived elsewhere (Ramanan and Brink, 1993).

Dye transfer assays

6-Carboxyfluorescein (6-CF, 376 Da, Molecular Probes, Eugene, OR) was dissolved in 120 mM potassium citrate (pH 9.0) to yield a final stock concentration of 20 mM and titrated to pH 7.0. Stock 6-CF solution was stored in the dark at −20°C. Microelectrode tips were backfilled with stock dye solution, and small N2A cell clusters (fewer than 10 cells) were impaled. The fluorescent probe filled the cell by simple diffusion. Typical filling times ranged from 30 s to 2 min. Impalements were monitored on the stage of an inverted microscope (Nikon Diaphot) by low light phase contrast and epifluorescent imaging. Epifluorescent illumination was provided by a 100 W mercury lamp power source and a 490 nm excitation filter. Photomicrographs were recorded on a Nikon 35 mm camera body attached to the microscope's camera port. Similar procedures were followed for the rhodamine dextran (10,000 Da) injections into high density N2A cell cultures.

For DWCR experiments using 6-CF, the 20 mM stock solution was diluted to a final concentration of 2 mM with IPS #1. Only one patch electrode was filled with the 2 mM 6-CF IPS #1, and junctional conductance measurements are obtained following normal procedures. After a specified junctional current recording period, the presence or absence of dye transfer was observed under epifluorescent illumination. Phase contrast and fluorescent micrograph images were recorded using an automatic exposure Olympus 35 mm camera body attached to the microscope's camera port.

For the fluorescein dextran (average M_r = 10,000) injections of low density cultures of N2A cells, cultures were trypsinized and plated at $\leq 10^5$ cells/60-mm dish. The cultures, 16–24 h later, consisted of primarily single cells and pairs of cells with a few larger clusters. Cell pairs were chosen for microinjection of a 100 mg/ml (in water) solution of FITC-dextran (average M_r = 70,000; Sigma Chemical Co., St. Louis, MO). Injections were performed by pressure injection using a Nikon pico-injector and were visualized with a Nikon Diaphot inverted microscope equipped with epifluorescence and Hoffman modulation contrast optics.

RESULTS

Conductance and gating properties of connexin-specific channels

The channel conductances (γ_j) of Cx37-specific channels were originally reported using a 110 mM Kglutamate pipette solution (IPS #1) in both patch electrodes of connexin-transfected N2A cell pairs. The maximum Cx37 γ_j of 219 ± 22 pS was determined from a total of 6 cell pairs and 139 channel openings obtained during a 2 min cumulative recording time (Reed et al., 1993). Conversely, the maximum γ_j was 94 ± 4 pS at $V_j > 80$ mV. Multiple channel conductances were reported but were not characterized further due to the complex gating activity observed in the multichannel recordings.

Single Cx37 gap junction channel activity was recorded at low transjunctional potentials using a 120 mM Kglutamate internal pipette solution (IPS #2) with 15 mM KCl and 10 mM TEACl added to both the external bath and internal pipette solutions. The increased ionic strength and addition of K^+ channel blocking ions should improve the signal-to-noise ratio of single channel currents by increasing the nonjunctional membrane resistance of the N2A cells and increasing the junctional channel current amplitudes. Analysis of channel activity from cell pairs that exhibited activity for only one Cx37 channel also improved the signal-to-noise ratio of single channel currents. Examples of Cx37-specific channel currents are illustrated in Fig. 1. The holding potential of cell 1 (V_1) was stepped from +25 to −25 mV as indicated by the arrow, whereas cell 2 (V_2) was held constant at 0 mV. Total whole cell currents for cells 1 and 2 (I_1 and I_2) are displayed and numerous transitions between three stable current levels (*solid lines* in I_2) are observed in this record (Fig. 1 *A*). All junctional current (I_j) activity is observed as simultaneous signals of equal amplitude and opposite polarity, although only the change in I_2 is used as a measure of I_j because I_1 contains both junctional and nonjunctional membrane current components associated with the voltage step. The amplitudes of the largest transitions measured 8.34 pA, or γ_j = 333 pS. Frequent transitions between the open state or ground state and an intermediate current state with an amplitude of 1.6 pA (γ_j = 64 pS) were also observed.

The current amplitude histogram, inclusive of the entire 90-s recording, was fitted with a probability density function (pdf) assuming two independent channel types corresponding to the above conductances (Fig. 1 *B*). The smaller channel accounted for 58% of the cumulative recording time, whereas the larger channel was open for only 9% of the cumulative recording time, as evidenced by the area under the corresponding peaks in the real time (all-points) histogram. The discrepancies between the actual data (*solid line*) and the pdf (*dashed line*) occur as a result of the assumption of independent channel types. The observed high open probability of the smaller channel predicts that its activity should appear superimposed on the less frequent openings of the

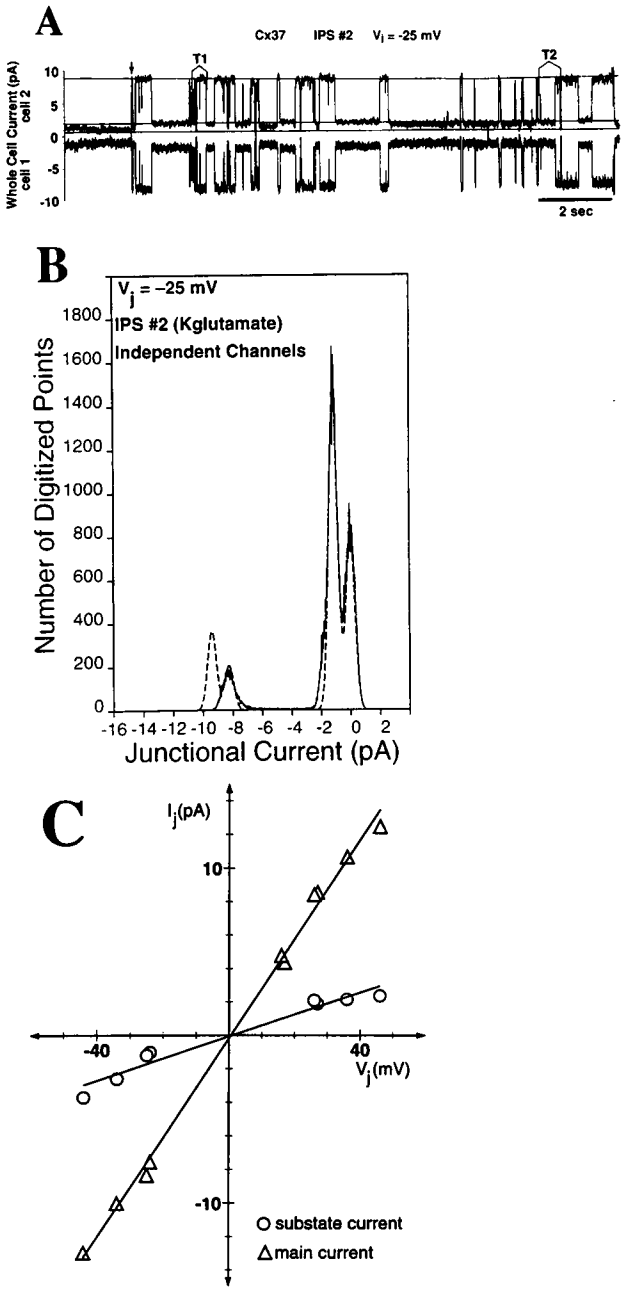

FIGURE 1 (*A*) Actual whole cell currents from a Cx37-transfected N2A cell pair using IPS #2. The holding potential of cell 1 (V_1) was stepped to −25 mV relative to cell 2 (V_2 = 0 mV), as indicated by the arrow, for 90 s to create a transjunctional potential (V_j) of −25 mV. All currents were low pass filtered at 100 Hz and digitized at a rate of 2 kHz. A 15-s segment of single channel activity is displayed that illustrates all three stable conductance levels evident in the amplitude histogram (*B*). The upper line indicates the main open state current, the middle line indicates the intermediate (substate) current level, and the bottom line indicates the ground state. (*B*) All points amplitude histogram compiled from the entire 90 s pulse interval. Junctional current (I_j) is taken as the inverse of the change in whole cell current of cell 2 because its membrane potential is held constant. All junctional currents are viewed as whole cell currents of equal amplitude and opposite polarity in cells 1 and 2. The solid line represents the actual digitized point count, and the dashed line is a mathematical fit (probability density function, pdf) of the Gaussian distributions. The fit assumes one closed state with a variance of 0.3 pA and two independent channel types with unitary conductances of 64 and 330 pS. The open channel variance was 0.3 pA. Open probabilities were 0.64 and 0.20, respectively. There were a total of 21 large channel events. The additional peak predicted above 9 pA results from the presence of the 64 pS channel in addition to the 330 pS channel. (*C*) Single channel current-voltage relationship for the Cx37 channel activity from the same N2A cell pair observed at various V_j values. The data were fit with lines having slope conductances of 297 and 65 pS (r > 0.97). The smaller conductance channel is termed a substate current because the activity of this channel was always observed to be intermediate between the closed and maximum open (~300 pS) states.

larger channel, as indicated by the additional peak in the pdf above 9 pA. High and low conductance states were observed in 1- to 2-min recordings at ±25, ±35, and ±45 mV (data not shown). The low conductance channel activity was never superimposed on the openings of the larger channel; rather, it always appeared as an intermediate current peak between the zero current and the maximum conductance channel peak in the amplitude histogram. The data from this experiment are summarized in the junctional single channel current-voltage (i_j-V_j) relationship (Fig. 1 *C*). All data points for the maximum (unitary) and intermediate (sub)conductance levels were determined from histogram fits of the cumulative recording period at each transjunctional potential (V_j). The i_j-V_j relationships for the unitary and subconductance states are linear with slope conductances of 297 and 63 pS. The SDs of the slopes are <±10 pS based on the signal-to-noise ratio. The intermediate conductance state was not observed at $V_j \leq \pm 20$ mV, and open probabilities and event counts for the maximum conductance state declined with increasing V_j. V_j pulses ≥±50 mV were not examined due to the complete lack of maximum open state channel events.

Multichannel recordings were obtained from two other Cx37 N2A cell pairs using IPS #2. The unitary and subconductance state slope conductances for the two active channels in one of these two experiments were 282 and 79 pS, respectively. An i_j-V_j relationship was precluded in the second experiment because only a few negative V_j pulses were obtained. The *two* channels in this cell pair exhibited a maximum unitary γ_j of 306 pS and substate γ_js in the range 60–80 pS at $V_j = -30$ mV. In both multichannel experiments, the 300-pS channel was not observed above ±45 mV; event counts <10 for the 300-pS channel at $V_j \geq \pm 30$ mV; and the intermediate 60–80 pS conductance state was not observed below ±20 mV during each 2 min recording period.

Subconductance state activity of Cx37 channels

Three hypotheses could explain the occurrence of multiple channel conductances observed in the Cx37 cell pairs: (i) distinct populations of independent channels with different conductances; (ii) cooperative gating of several identical channels to yield apparently higher conductances; or (iii) subconductance states of a large conductance channel (Chen and DeHaan, 1992). The demonstration of a channel substate requires observation of the concomitant activity of low and high conductance states that directly interconvert and cannot be accounted for by the superposition of two independent channels (Fox, 1987).

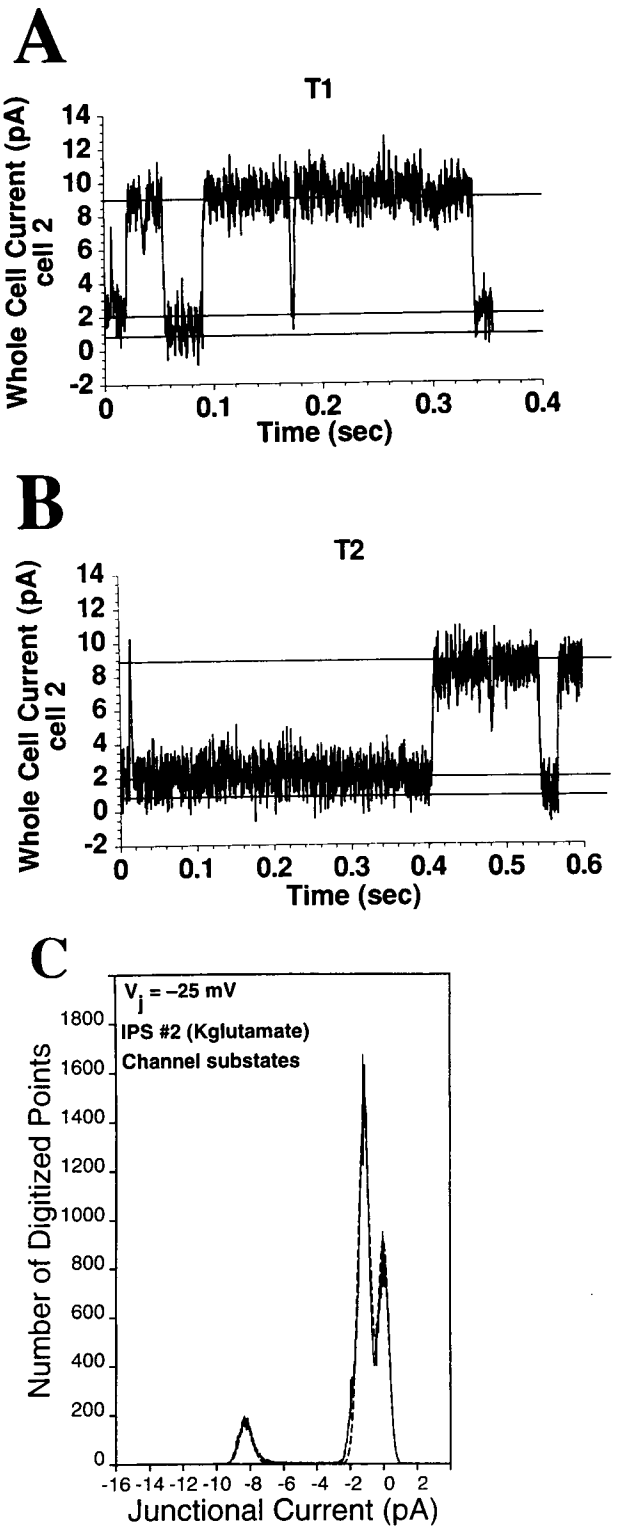

FIGURE 2 (*A*) Cell 2 whole cell currents were redigitized at 10 kHz after low pass filtering at 1 kHz. A 350-ms interval (T1 in Fig. 1) is illustrated that depicts rapid transitions from the substate to maximum open state and maximum open to ground state transitions. (*B*) A similar 1-kHz signal from a second (T2) time interval displayed in Fig. 1. Notice that the brief, rapid opening in this figure reaches the full amplitude of the fully open channel in this record. (*C*) All points amplitude histogram fitted with a pdf that assumes the presence of one open 330-pS channel and a 46-pS substate of this same channel. The evidence for direct, rapid interconversions between the two conductance states and the improved amplitude histogram fit over the independent channels pdf in Fig. 1 are indicative of substate channel activity for the Cx37 channel. Note that the subconductance state predominates even at low voltages.

The pdf in Fig. 1 *B* was generated assuming distinct populations of independent channels, and the apparent discrepancies with the actual current amplitude distribution provides a strong statistical argument against this hypothesis. As stated above, the discrepancies between the experimental current amplitude distributions and the independent channel pdfs result from the experimental observation that the low conductance channel activity always appeared as an intermediate current peak between the zero current and the maximum conductance channel peak in the amplitude histogram. The cooperative gating of smaller channels to produce a higher conductance channel is unlikely given the high open probability of the 63 and 80 pS channel states, the low open probability of the 300 pS channels, and the absence of any other intermediate conductance levels between these two conductance states.

The direct interconversion between the three observed Cx37 channel conductance states (maximum open, closed, and intermediate) are best resolved at filter frequencies higher than those illustrated in Fig. 1. For this purpose, the current traces displayed in Fig. 1 were low pass filtered at 1 kHz and resampled at 10 kHz. Two time points, labeled T1 and T2 in Fig. 1 *A*, are redisplayed in Fig. 2, *A* and *B*. The incomplete closure in T1 and incomplete opening in T2 between the maximum and intermediate conductance states now appear as full amplitude interconversions between these two states. Other fully resolved maximum open-closed transitions are readily resolved in Fig. 1 *A* and Fig. 2, *A* and *B*, although the signal-to-noise ratio between the closed and subconductance states is reduced at the higher filter frequency.

The substate hypothesis is strongly favored based on the above findings and because the low conductance channels always occurred in the presence of the large channel, albeit sometimes for prolonged intervals of several seconds. As a final test of the channel subconductance state interpretation, the current amplitude histogram was fitted with a second pdf that assumes that a given channel has x substates of y amplitude (Ramanan and Brink, 1993). The pdf illustrated in Fig. 2 *C*, which was generated assuming that the intermediate current peak is a single substate of the fully open channel, provides a more accurate fit of the experimental data than was possible for the independent channel model (Fig. 1 *B*). All of the above evidence is consistent with the interpretation that the 63-pS channel is a substate of the fully open 300 pS Cx37 channel and provides a more rigorous test of the three criteria for substates than previously demonstrated for any expressed connexin-specific or native gap junction channel.

Chloride permeability of Cx37 channels

To examine the anion permeability of the Cx37 channels, channel current amplitudes were determined in separate

experiments using a modified internal pipette solution (IPS #3) where 120 mM KCl replaced Kglutamate as the major monovalent ions. In one single-channel experiment, channel currents were recorded at 10 different V_js. Fig. 3 *A* is a 15-s segment of the paired junctional channel currents obtained during a 2 min V_j pulse to −30 mV. Numerous transitions between three stable (closed, substate, and maximum open) conductance states are observed. The T1 time point is redisplayed in Fig. 3 *B* to illustrate the direct interconversions between all three conductance states at a higher temporal resolution (1 kHz filter frequency). The current amplitude distribution for the entire 2 s recording interval is shown in Fig. 3 *C* and is fitted with the independent channel model pdf. Although less obvious in this example because of the lower cumulative open times for both the unitary open and substate activity at this higher V_j, the pdf again predicts a low level of channel activity to be superimposed on the fully open channel (see *inset*), which was not observed experimentally. Fig. 3 *D* is the same real time amplitude histogram fitted with the substate pdf to illustrate the improved fit of the actual data. All of these observations are consistent with the previous experiment using IPS #2 and again illustrate the substate channel activity of the Cx37 gap junction channel.

Taking into account the fivefold increase in Cl^- concentration between IPS #2 and #3, one would predict a 38% increase in junctional channel current and conductance, assuming that the permeabilities of the pertinent ions (K^+, Cs^+, TEA^+, glutamate$^-$, and Cl^-) are directly proportional to the

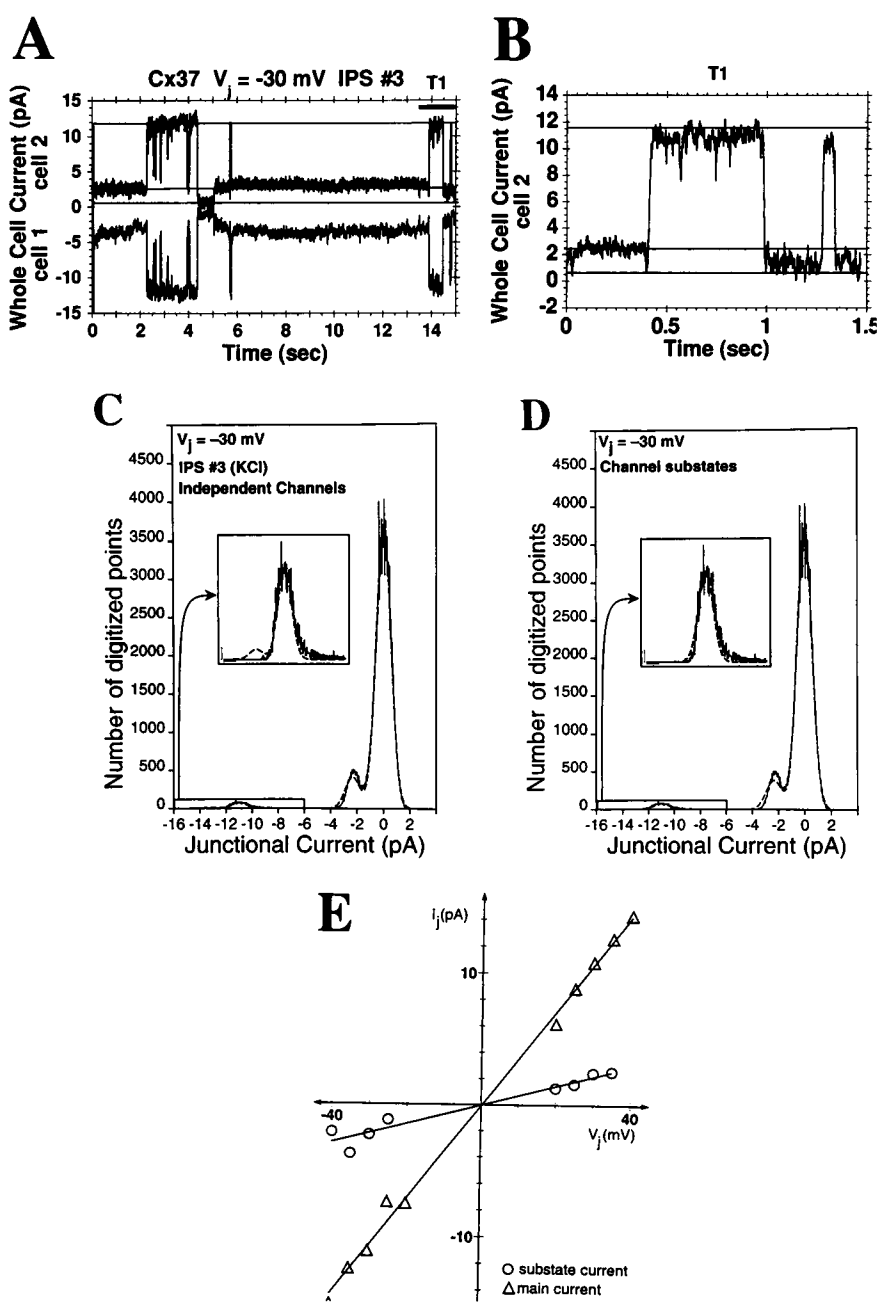

FIGURE 3 (*A*) Whole cell currents from a second Cx37-transfected N2A cell pair using IPS #3. Experimental procedures are similar to those presented in Fig. 1. The onset of the pulse is indicated by the brief channel opening at time zero. Again, two distinct conductance levels and a closed state are observed, this time at a V_j of −30 mV. (*B*) High frequency record of a brief channel current interval (T1) displayed in *A*. Direct, rapid transitions from the substate to ground state and ground to open states are observed. These results again illustrate the existence of at least one substate of the fully open Cx37 channel. (*C*) All points amplitude histogram compiled from the entire 120 s junctional current record. The pdf assumes one closed state with a variance of 0.4 pA and two independent channel types with unitary conductances of 78 and 370 pS (variance = 0.4 pA). Open probabilities were 0.12 and 0.03, respectively. There were a total of 12 large channel events. The additional peak predicted below −12 pA assumes the presence of the 78 pS channel in addition to the 370 pS channel. (*D*) All points amplitude histogram fitted with a pdf that assumes the 78-pS channel is a substate of the 370-pS channel. (*E*) Junctional channel current-voltage relationship for the Cx37 channel and substate in 120 mM KCl internal pipette solution. The slope conductances were 357 and 73 pS ($r > 0.97$). The differences in the slope conductances of the Cx37 open state and substate channels correlates with an effective Cl^-/K^+ permeability of 0.43 for the maximum open state and 0.3 for the substate.

aqueous mobilities of the ions. The slope conductances for the maximum unitary and substate conductances were 357 and 73 pS, respectively. The open channel noise was similar to records obtained using IPS #2. Hence, The SDs of the slopes are again $<\pm 10$ pS. This amounts to only a 20% increase in γ_j for the maximum open state of the Cx37 channel and 16% increase in γ_j for the 63-pS substate, based on single-channel current records. The 20% increase in maximum γ_j constitutes only a 53% increase relative to the expected value, assuming that the local ion concentrations near the mouth of the Cx37 channel are equal to their respective values in the IPS and the permeabilities reflect the aqueous mobility of each ion in solution. From our initial estimates, using the Goldman-Hodgkin-Katz current equation, this experimental conductance ratio can be achieved by lowering the relative anion/cation permeability to 0.43. An electrostatic field near the mouth of the pore, which effectively increases the local cation concentration by 53% and reciprocally decreases the local anion concentration, can also account for only a 20% increase in channel conductance.

Multichannel recordings were also obtained from two other Cx37 N2A cell pairs using IPS #3. The unitary and subconductance state slope conductances for the active channels in both of these experiments were 344, 341, 92, and 52 pS, respectively. In a third experiment using 140 mM CsCl and 15 mM TEA IPS (10% higher osmolarity), the maximum unitary channel conductance increased to 373 pS at $V_j = -30$ mV (data not shown; Veenstra et al., 1993). All of the multichannel data are consistent with the findings from single-channel records of a lower than predicted IPS #3/IPS #2 conductance ratio for the maximum open state of the Cx37 channel. The data regarding the subconductance state are presented based on the measurements of a predominant subconductance state from the single channel records, whereas the subconductance state γ_j data from multichannel experiments are more variable and may indicate the presence of more than one substate for the Cx37 channel.

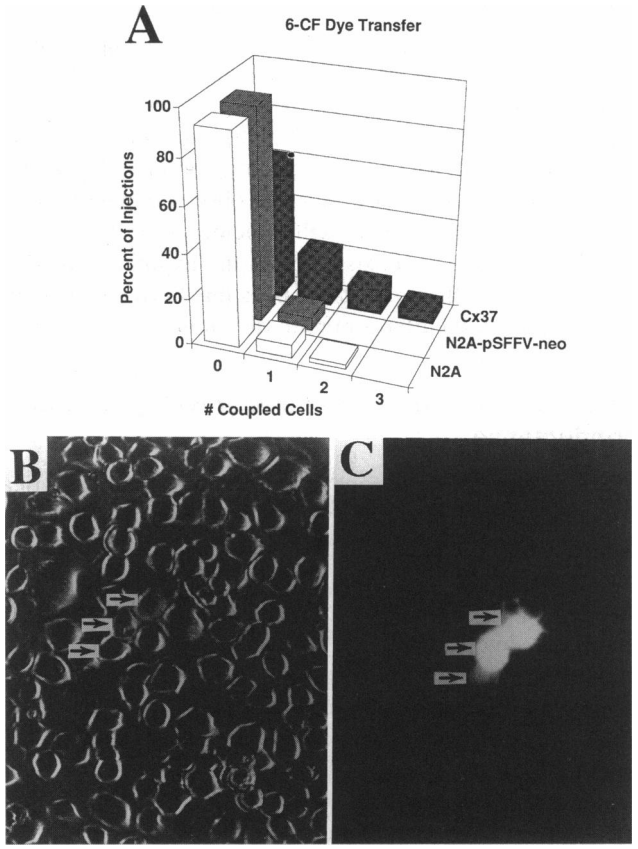

FIGURE 4 (*A*) Distributions of dye-coupled cells in nontransfected, vector-transfected, and Cx37-transfected N2A cell clones. N2A cells were grown to near confluence and impaled with a microelectrode backfilled with 120 mM Kcitrate plus 20 mM 6-carboxyfluorescein, pH 7.0. The fluorescent probe filled the cells by simple diffusion. Filling times ranged from 30 s to 2 min. Observation times ranged from 2 to 10 min. The incidence of dye transfer to one or more cells in the two control groups was <8%, but was 36% in the Cx37-transfected N2A cells. (*B*) Phase contrast micrograph of Cx37-transfected N2A cells after 2 days in culture. The 15 μm diameter cell indicated by the center arrow was impaled with a dye filled electrode for 1.5 min. (*C*) Fluorescent image of the same field taken 2.25 min after the onset of impalement. One neighboring cell (*top arrow*) fluoresced with similar intensity to the injected cell, whereas a distinct dye diffusion gradient is evident in the second coupled cell (*bottom arrow*).

6-CF dye transfer in connexin-transfected N2A cell cultures

To examine the dye permeability of the channels, 6-CF was injected into near confluent monolayers of N2A cells. This anionic dye was selected because of its molecular weight ($M_r = 376$) and hydrophilic character. Dye transfer was observed in 4 of 52 (7.7%) injections in cultures of untransfected N2A cells and 4 of 99 (4.0%) injections in vector-transfected N2A cells (transfected with the pSFFV-neo eukaryotic expression vector without any connexin cDNA insert; Veenstra et al., 1992). In contrast to N2A control groups, dye transfer was observed in 35.7% ($n = 98$) of Cx37-transfected N2A cells with occasional dye transfer to two or three coupled cells (Fig. 4 *A*). A majority of the positive 6-CF coupled cells in N2A and vector-transfected N2A cells fluoresced rapidly (within 15 s) and with equal intensity to the injected cell. Rapid fills accounted for only 40% of the dye-coupled Cx37-transfected N2A cells. In the remaining 22% of the Cx37 dye injection experiments, dye transfer was observed to develop gradually over a period of 1–10 min with obvious 6-CF concentration gradients between the primary injected and neighboring cells (Fig. 4, *B* and *C*). The incidence of electrical coupling, determined from separate DWCR experiments, was 66% for Cx37 N2A cell pairs ($N = 88$).

One possible explanation for the low incidence of rapid dye transfer in all three experimental groups is that the neighboring cell was nonspecifically coupled to the primary injected cell by cytoplasmic bridges. To examine the hypothesis that these cells were connected by cytoplasmic bridges, rhodamine dextran (average $M_r = 10{,}000$) was injected into near confluent monolayers of vector-transfected N2A cells. Dye transfer was observed in 2 of 24 injections (8.3%) and occurred in both isolated cell pairs and small clusters of <10

cells. The incidence of dye transfer with rhodamine dextran in the vector-transfected N2A cells is nearly identical to the basal level of dye transfer observed in untransfected N2A cells with 6-CF. The hypothesis was further examined by injecting FITC-dextran (M_r = 70,000) into pairs of untransfected N2A cells plated at low density to mimic the DWCR culture conditions. Dye transfer was observed in 6 of 46 cell pairs (14.6%, Fig. 5). The higher incidence of dye transfer in N2A cell pairs is consistent with the hypothesis that the 6-CF positive cells are daughter cells that have not yet completed cytokinesis after a mitotic division.

Direct correlation of dye transfer with junctional conductance

To correlate the occurrence of dye transfer with electrical coupling, DWCR experiments were performed on pSFFV-N2A and Cx37-N2A cell clones with 2 mM 6-CF added to one of the recording pipettes (IPS#1). Low levels of endogenous coupling analogous to that observed in the SKHep1 cell line (Moreno et al., 1991a) were never observed in 50 vector-transfected N2A cell pairs. However, pSFFV-N2A cell pairs with a high junctional conductance (g_j = 13–32 nS, 23 ± 6 nS = mean ± SD) and lacking any demonstrable sensitivity to transjunctional potentials, heptanol, or acidification to pH ≤ 6.0 were observed in 26% of the experiments. The incidence of high g_j nonspecific coupling ranged from 10 to 40% for all control and experimental (connexin-transfected) N2A cell cultures examined. All of these high conductance cell pairs also exhibited 6-CF dye transfer with characteristic bright intensity equal to the primary injected cell, consistent with the above interpretation of cytoplasmically fused or dividing cells. In all of our experiments in control or vector-transfected N2A cells, low conductance cell pairs with quantal currents characteristic of endogenous channel activity were never observed. To avoid inclusion of the high conductance, nonselective coupled cells in the Cx37 DWCR dye transfer experiments, only those pairs with demonstrable g_j < 20 nS, V_j dependence or g_j blockade by 2 mM heptanol were counted in the final analysis.

6-CF dye transfer was observed in one 3.8 nS Cx37-transfected N2A cell pair where 200-pS channel (219 ± 22 pS in IPS #1; Reed et al., 1993) activity could also be demonstrated (Fig. 6 *A–C*), which assumes a maximum of 19 fully open Cx37 channels. Overall, similar dye transfers were observed in 7 of 28 Cx37 experiments, including two unexpected occasions where distant cells (>40 μm) made contact with the primary injected cell only through neurite outgrowths, which precluded the direct measurement of junctional conductance. The ability of Cx37 channels to pass 6-CF may depend on the conductance state of the channel,

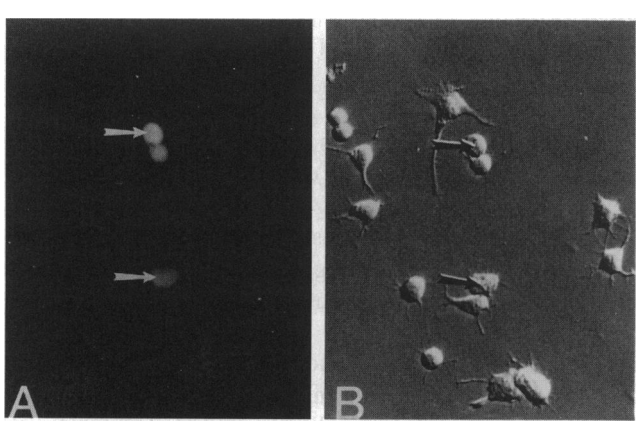

FIGURE 5 Intercellular passage of high molecular weight fluorescent tracers in N2A cells. One day after nontransfected N2A cells were plated at low density, single cells in pairs were injected (*arrows*) with FITC-dextran (average M_r 70,000). Cells were visualized by epifluorescence (*A*) or Hoffman modulation contrast (*B*) optics. In many cases, dye remained only in the injected cell, but dye transfer to the partner cell was observed in 15% of the injections.

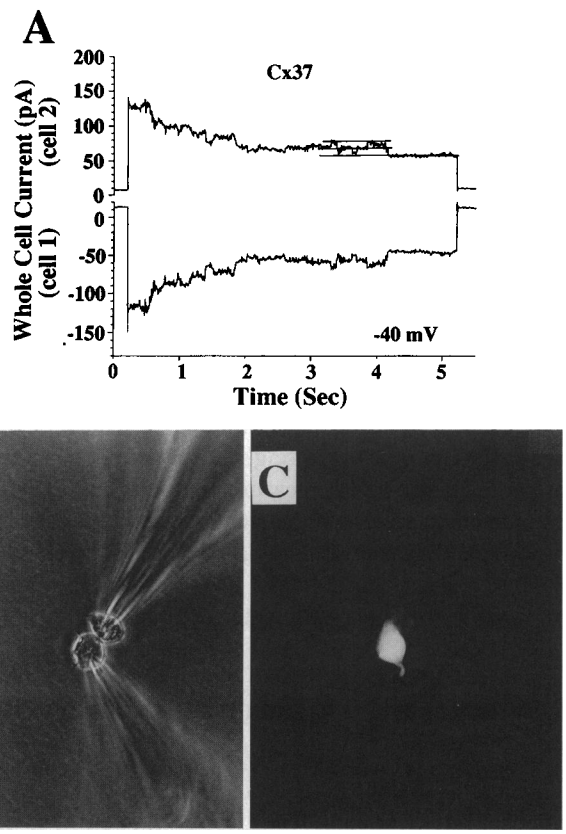

FIGURE 6 Simultaneous determination of macroscopic junctional conductance and 6-CF dye transfer in Cx37-transfected N2A cell clones. (*A*) Paired whole cell currents from a Cx37-transfected N2A cell pair during a train of −40 mV V_j pulses. Five s voltage steps from 0 to −40 mV were applied once every 15 s. Only a single pulse is shown to provide temporal resolution of 8 pA (200 pS) channel activity observed during the pulse (*solid lines*). The instantaneous and steady state g_j for the 5 min recording period were 3.8 and 1.5 nS. (*B*) Phase contrast micrograph of the same Cx37-transfected cell pair in the DWCR configuration immediately after cessation of a 5 min recording period. The lower electrode contained 2 mM 6-CF in IPS #1. (*C*) Epifluorescent micrograph of the same cell pair taken immediately after detachment of the patch electrodes to remove the 6-CF dye filled electrode from the exposure field. This was necessary to optimize the image of the dye-filled cells. Dye transfer was evident in cell 2 before and after removal of both patch electrodes. Note that a dye diffusion gradient is still evident in this cell pair.

because dye transfer was not observed in several Cx37-transfected N2A cell pairs with g_j ranging from 0.75 to 15.8 nS (mean g_j = 7.2 ± 4.6 nS, n = 28). In all DWCR experiments, including the examples shown in Figs. 1 and 3, the open probabilities of the large Cx37 channel was <0.30 for $V_j \leq 30$ mV and diminished (sometimes to zero) in favor of the lower conductance state during the recording period. Open probabilities were reduced to zero when $V_j \geq 50$ mV. Recovery intervals of V_j = 0 mV did not restore the large channel activity in these instances, although reversing the polarity of the V_j pulses often did restore large channel activity in the same cell pair. These results suggest that low prolonged V_j pulses might affect the conductance state of the Cx37 channels. In our DWCR dye transfer experiments, the cells were exposed to a 40 mV V_j for 33% of the observation time to monitor g_j. 6-CF dye transfer was observed in cell pairs where 200 pS channel activity could be demonstrated, although it is not possible to ascertain the conductance state of all the channels in a given cell pair.

Because 6-CF is an anionic dye, it is possible to affect electrophoretically the rate of dye transfer across the gap junction. We examined the effect of reversing the electric field on the single channel γ_j using IPS #3 with 2 mM 6-CF added to one patch pipette. Hyperpolarizing and depolarizing V_j pulses were applied to the dye-containing cell of a Cx37 N2A cell pair for a duration of 2 min. As before, in the absence of any 6-CF dye, two prominent conductance states were observed (Fig. 7). For the examples presented in Fig. 7, *A* and *B*, the maximum unitary γ_j was 343 pS and the substate γ_j was 85 pS at V_j = +35 mV. Depolarizing pulses applied to the 6-CF-containing cell will favor containment of the dye in the primary injected cell. When the opposite polarity V_j is applied to the 6-CF containing cell, dye transfer is favored and maximum unitary and substate γ_js of 307 and 54 pS were observed (V_j = −30 mV). The current amplitudes for the maximum unitary and substate currents are summarized in Fig. 7, *E* and *F*. The slope conductance of the maximum (main) channel for all voltages was 350 pS (r = 0.99). Independent linear regression analysis of the channel current amplitudes at positive and negative voltages produced slope conductances of 350 and 274 pS ($r \geq 0.95$), a 22% decrease in the unitary conductance. The linear correlation of the substate currents is less reliable (r = 0.89) with a slope conductance of 96 pS.

A second single channel experiment under similar experimental conditions yielded slope conductances of 356 and 271 pS for the respective dye-trapped and dye-transfer voltage polarites, a decrease of 24% in γ_j. Substate current amplitudes could not be determined accurately in this experiment. The decrease in amplitude of the maximum unitary channel state is interpreted as a partial block, relative to the free ion-conducting state, of the channel by the permeant dye molecules. Whether the dye molecules may pass through the subconducting state of the channel cannot be determined reliably from these results. Regardless, these results provide the first conclusive evidence of dye-channel interactions during dye transfer and may partially explain the low incidence of dye coupling observed in the presence of the high conductance Cx37 channels.

DISCUSSION

Characterization of substate channel activity in gap junction channels

Previous experimental results have shown that the connexins form gap junction channels with distinct conductance and gating properties (Veenstra et al., 1992; Reed et al., 1993; Rup et al., 1993; Fishman et al., 1991; Moreno et al., 1991a). The data presented here provide the first definitive evidence of subconductance state activity, differential ion selectivity, and dye permeability of gap junction channels formed by a distinct connexin. The multiple channel conductances observed in junctional currents from 7-day embryonic chick heart, chick connexin42, and chick and human connexin43 isoforms (Chen and DeHaan, 1992; Moreno et al, 1992; Veenstra et al., 1992) are proposed to result from the occurrence of subconductance states. Substate activity is best defined by three criteria: (i) a channel substate should interconvert with the main channel state; (ii) substate activity should be observed only in the presence of the main channel state; and (iii) one must exclude the possibility that the different states arise from the superposition of two independent channels (Fox, 1987). These criteria were not applied to the previously published examples of multiple channel conductances. Recently, new methodologies for demonstrating the presence of subconductance states were developed (Ramanan and Brink, 1993) and applied to our double whole cell Cx37 channel recordings. All three substate conditions are met by the observed Cx37 channel activity (Figs. 1–3 and 7), and the independent and substate channel pdfs of the amplitude histogram provide the strongest evidence that the observed channel activity does not result from the behavior of independent channel types. In all of these instances, the favored channel state is not the maximum open (main) channel state but the subconductance state. This substate interconversion is favored by voltage because the cumulative open time and event counts of the 300-pS channel were observed to decline with increasing transjunctional potentials. High V_j and low temperatures are known to reduce the γ_j of embryonic chick cardiac gap junctions (Chen and DeHaan, 1992, 1993).

There are indications of other possible Cx37 channel substates that have not been presented in any detail here. Two different substate conductances of 63 and 80 pS were observed in the multichannel recordings using IPS #2, and for all experiments performed during the course of this study, subconductance state values range from 50 to 90 pS. The best illustration from the existing single-channel data is in Figs. 1 *B* and 2 *B*, where the current amplitude histograms exhibit a small peak that cannot be defined without assuming a third independent channel type or second substate in the two different pdfs. There is some indication of slightly different amplitude subconductance states in the dual current traces illustrated in Fig. 1 *A*. Similar current amplitude histograms

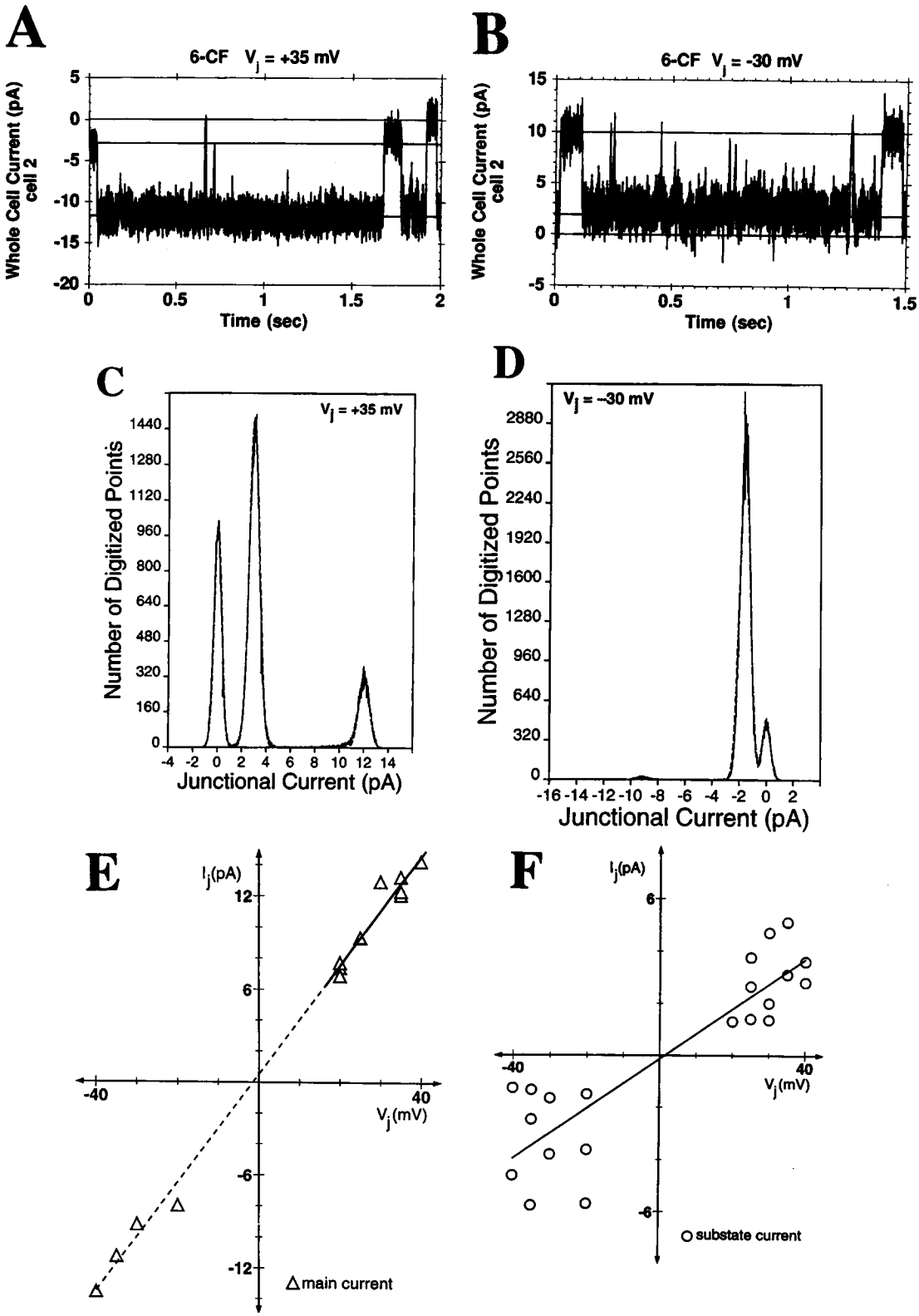

FIGURE 7 Effect of 6-carboxyfluorescein on Cx37 single channel conductances. (*A*) 2 mM 6-CF was added to cell 1, and a 2 min depolarizing voltage pulse was applied to produce a V_j = +35 mV, thereby trapping the anionic dye in cell 1. A 2-s segment of junctional channel current activity filtered at 1 kHz illustrates the rapid current transitions between the open, subconductance, and closed states of the Cx37 channel. (*B*) A similar 2 s high frequency channel current record from cell 2 during a −30 mV hyperpolarizing pulse, which favors dye transfer to cell 2. (*C*) All points amplitude histogram of the entire 2 min +35 mV V_j pulse (100 Hz filter) fitted with the substates pdf assuming the presence of a single 85 pS substate (open probability = 0.58) of the 343 pS open channel (open probability = 0.13). Closed variance was 0.31 pA, and the additional open variance was 0.28 pA. (*D*) All points amplitude histogram and substate pdf obtained from the same cell pair during the 2 min −30 mV V_j pulse (100 Hz). The open probabilities were 0.87 for the 54 pS substate and 0.007 for the 307 pS open state. Closed and open variances were 0.31 and 0.24 pA, respectively. (*E*) Open channel current i_j-V_j relationships

were observed at different voltages for the experiment shown in Fig. 7 (data not shown). The occurrence of other Cx37 channel substates are either too infrequent or of low amplitude to be readily resolved from the 2 min whole cell current records obtained from this investigation. The true test of whether there are multiple subconductance states to the Cx37 channel will come from longer stationary current recordings and an improved signal-to-noise ratio as performed on earthworm median giant axon junctional membranes (Brink and Fan, 1989; Ramanan and Brink, 1993).

Ionic selectivity and conductance of gap junction channels and a reevaluation of the simple pore model

The Kglutamate/KCl ion substitution experiments (Figs. 1 and 3) provide the first direct evidence for a reduced anionic conductance of a high conductance gap junction channel. The aqueous nature of the gap junction pore was best illustrated by the D_2O effects on g_j in the median giant axon junctional membrane (Verselis and Brink, 1986). According to the simple pore model, the aqueous mobilities should determine the monovalent ion selectivity sequence. Based on the relative aqueous mobilities of all permeant ions ($K^+ = 1$, $Cs^+ = 1.05$, $TEA^+ = 0.44$, $Cl^- = 1.04$, and glutamate$^- = 0.36$), a 38% increase in maximum γ_j of the Cx37 channel was expected with the substitution of IPS #3 for IPS#2. One possible explanation for the experimentally observed 20% increase in γ_j is to assign a relative anion/cation permeability of 0.43, which reduces the relative glutamate$^-/K^+$ and Cl^-/K^+ permeabilities to 0.15 and 0.45, respectively. Given the experimental variability in the γ_j measurements due to the open channel variance and range of γ_j values obtained with each IPS, the IPS #3/IPS #2 conductance ratios may range from 1.12 to 1.25. The corresponding relative anion/cation permeability estimates for the Cx37 channel range from 0.32 to 0.66. It is interesting that our Cx37 channel data agree closely with previous relative Cl^-/K^+ conductance and permeability estimates of 0.52–0.69 from rat lacrimal gland cell and earthworm median giant axon gap junction channels with diverse protein compositions (Neyton and Trautmann, 1985; Brink and Fan, 1989).

Assuming a channel length of 18 nm and resistivity of 100 Ω-cm, values that provide a maximum γ_j estimate for a gap junction channel, a Cx37 channel (220 pS in IPS #1) requires a channel diameter of 22–23 Å. This projected diameter of the Cx37 channel is 50% higher than the estimated diameter of mammalian cell gap junctions derived from classical morphological evidence (Makowski et al., 1984). The relative anion/cation permeability ratio of 0.43, the effects of 6-CF on γ_j, and the low incidence of 6-CF dye transfer in Cx37-transfected N2A cell pairs are also inconsistent with a molecular sieve selectivity filter of these physical dimensions. A second possible mechanism that could explain the high maximum unitary and low relative anion/cation conductances of the Cx37 channel would be the presence of a negatively charged electrostatic field near the mouth of the pore. Rings of acidic amino acid residues near the mouth of the nicotinic acetylcholine receptor channel pore are known to influence the degree of Mg^{2+} block, channel conductance, and cationic selectivity of this ligand-gated channel (Imoto et al., 1988). Although other amino acid residues are also important in determining the cation selectivity sequence of the nicotinic acetylcholine receptor channel, the net charge of the anionic ring closest to the narrowest portion of the channel was found to have the greatest effect on channel conductance, consistent with the formation of an electrostatic barrier.

Implications of selective permeability and multiple conductance states on intercellular signaling

Subconductance states, low maximum open channel probabilities, and low anion conductances of Cx37 channels may have obvious functional consequences upon the spread of electrotonic potentials in intact tissues (e.g., endothelium). Thus, the gating and permeability properties of connexin-specific gap junction channels will also modulate the forms of biochemical signaling that can occur between cells. Lucifer yellow dye transfer studies have often been used to assay for the presence of functional gap junctions in a variety of cell and tissue preparations (Kolb and Somogyi, 1991), but only a few of these studies have considered the role of channel gating and permeability on dye transfer. Ignoring for the moment the relative contributions of the cytoplasm to intercellular fluorescent dye transfer (Safranyos et al., 1987), there are at least three criteria that must be met if the presence or absence of dye transfer is to be considered a reliable indicator of functional gap junctional communication.

The first criterion that must be addressed is whether the observed dye transfer occurs through functional gap junctions. We have made the distinction between functional dye and electrical coupling produced by connexin expression and the low incidence of high conductance and permeability produced by putative cytoplasmic bridges based on several criteria. The electrical coupling produced by most functionally expressed connexins (Cx26, Cx32, Cx37, Cx38, Cx42, Cx43, Cx45) exhibit some degree of transjunctional voltage dependence and reversible blockade by 1-alkanols, halothane, or low pH (Ebihara et al., 1989; Fishman et al., 1990; Moreno et al., 1991a, b; Rubin et al., 1992; Veenstra et al., 1992; Reed et al., 1993). The same criteria were applied to the g_j measured between C6/36 cells, a cell line dervied from *Aedes*

for the above experiment. Linear regression analysis (*solid line*; $r = 0.96$) of the positive V_j values produced a slope conductance of 350 pS. The dashed line is the projected fit of all data points assuming a slope conductance of 350 pS. Linear regression analysis of the negative V_j values yielded a slope conductance of 274 pS (not shown; $r = 0.95$), a 22% reduction in γ_j in the direction favoring dye transfer. (*F*) Substate channel current i_j-V_j relationship for the same cell pair. The slope conductance is 96 pS ($r = 0.89$).

albopictus, to demonstrate the presence of functional gap junctions (Bukauskas et al., 1992). In 21% of the cell pairs they examined, g_j was insensitive to all of the above treatments and the mean g_j was approximately 4 times higher (~20 nS) than the previous experimental group. Partial blockade with supramaximal (3 mM) doses of 1-heptanol was observed in 13% of the C6/36 cell pairs, consistent with the coexistence of functional gap junctions and cytoplasmic bridges. Putative cytoplasmic bridges have also been observed in other vertebrate and insect cell lines (Flagg-Newton et al., 1981; Spray et al., 1989) and have been attributed to incomplete cytokinesis after a mitotic division, which manifests itself by the presence of a narrow bridge (the midbody) in the cleavage furrow between daughter cells (Karasiewicz et al., 1981).

We have functionally expressed five different connexins in the N2A cell line (Veenstra et al., 1992; Reed et al., 1993; Rup et al., 1993). Chick connexin42, connexin43, connexin45, and human Cx37 all exhibited voltage- and heptanol-sensitive g_j with mean values of 3–6 nS, with Cx56 being the lone exception to this observed behavior. We routinely excluded all N2A cell pairs from the above electrophysiological examinations, which exhibited voltage- and heptanol-insensitive g_js (8–35 nS). Thirteen of fifty vector-transfected N2A cell pairs exhibited similar voltage- and heptanol-resistant g_js (mean $g_j = 23 \pm 6$ nS). In contrast to the Cx37 DWCR 6-CF dye transfer experiments, all of the electrically coupled vector-transfected N2A cell pairs were also brightly dye-coupled. Our findings in the vector- and connexin-transfected N2A cell clones are entirely consistent with the occasional occurrence of cytoplasmic bridges between cells. As an additional test of this hypothesis, 10-kDa rhodamine dextran or 70-kDa FITC dextran conjugates were injected into near confluent monolayers or pairs of vector-transfected N2A cells. The incidence of dye transfer was demonstrated to be similar to the observed rate of dye-coupling in control N2A, vector-transfected N2A, and treatment-resistant high g_j Cx37 N2A experimental groups. Although the high molecular weight dextran polymers are normally distributed around a mean of 10 or 70 kDa, this 10-kDa rhodamine-conjugated dextran polymer has been demonstrated to not diffuse across Lucifer Yellow permeable gap junctions in cultured monolayers of mammalian cells (El-Fouly et al., 1987; Mantz et al., 1993). Combined with the experimentally measured rate of nonspecific dye transfer in vector-transfected N2A cell pairs, determination of functional electrical coupling, and lack of 6-CF dye transfer in our Cx37 N2A cells, we have concluded that the low incidence (5–8% in monolayers, 20–26% in cell pairs) of dye transfer observed in all N2A cell experimental groups can be attributed to the presence of direct cytoplasmic continuity between cells.

A second condition that must be demonstrated is whether the expressed connexin-specific gap junction channel is permeable to the chosen tracer molecule. Because all commonly used hydrophilic fluorescent tracer molecules are negatively charged, as are many of the physiologically relevant second messengers (e.g., cAMP, IP_3), the relative anion/cation permeability of the channel becomes an important consideration. Cationic dyes with similar permeability properties to the fluorescein derivative used here would be ideal for examining the permeability of relatively cation-selective gap junction channels. Suitable candidates remain to be identified. Future experiments will be directed towards further examination of the cationic permeability of the Cx37 channel.

It is also possible that the pore size and, therefore, the molecular permeability limit vary with the conductance state of the channel. Our experimental data indicate that permeant dye molecules nearing the putative physical dimensions of the pore interact with the channel to reduce effectively the ionic conductance of the fully open channel, perhaps by temporarily increasing the channel transit time or converting the channel to a single-file pore. Gap junction channel subconductance states may not even be permeable to similar anionic 10–12 Å diameter molecules, thereby serving to convert the gap junction channel to a moderately selective ion channel.

A final consideration in the applicability of dye transfer experiments as an assay for the presence of functional gap junction channels is one of detection. If a gap junction is capable of passing a 100 picocoulomb/s ($\approx 10^9$ ions/s) through 20 open 200-pS channels (Fig. 6 *A*), an estimated relative dye/K permeability of only 0.001 should result in the passage of 10^6 dye molecules/s. Assuming a 6-CF detection limit of 1–10 μM, a cell volume of 1 pl (15-nm-diameter cell), and a 6-CF concentration of 1 mM in the primary cell ($\approx 10^8$ molecules), 6-CF dye transfer should become detectable in the partner cell within 1–10 s once the dye reaches the channels. So it is feasible to detect 6-CF dye transfer using the DWCR technique reported here (Fig. 6 *C*). However, these projections assume that the steady-state g_j of a Cx37 cell pair is comprised of a homogeneous population of fully open channels. In our observations, the open probability of any Cx37 channel rarely exceeded 0.20 even at $V_j \leq \pm 20$ mV, making the preceeding conditions highly improbable. If the Cx37 channel subconductance state is not dye-permeable, then detectable dye transfer would depend entirely upon the cumulative open time of the maximum unitary channel conductance state. Under conditions where the open probability of the dye permeable channel conductance state is reduced, the time required for detectable dye transfer could be increased indefinitely. It should be noted that the standard microelectrode and DWCR dye injection results are not necessarily analogous because intracellular cell dialysis by the IPS may alter the gating properties of the channel. The apparent discrepancy in the incidence of dye and electrical coupling can be accounted for by the differential permeability properties associated with the different conductance states of the connexin channel, detection limitations, intracellular dialysis, or any combination of these circumstances.

In conclusion, our experimental results demonstrate that Cx37 gap junction channels exhibit distinct unitary and subconductance states, an effective anion/cation permeability ratio of 0.43, and a reduction in unitary conductance during transfer of 6-CF fluorescent dye molecules that approaches

the permeability limit of the hydrophilic pore. These characteristic channel properties have not been demonstrated for any other gap junction channel to date and are not consistent with the classical interpretation of the gap junction channel as a simple, two-state aqueous pore. Instead, the gating, conductance, and selectivity properties of the Cx37 channel exhibit many features common to many other more conventional ion channels. Future experiments designed to examine the permeability properties and structure-function relationships of multistate connexin-specific channels should provide insight into the molecular mechanisms underlying the basis for the newly appreciated differences in intercellular signaling that occur through connexin-specific gap junction channels.

This work was conducted with the technical assistance of M. Chilton, E. Westphale, and B. Grine. We wish to thank Dr. Andrew L. Harris for helpful discussions on the relative ion permeabilities of connexin channels.
This work was supported by grants HL-45466, HL-42220, and HL-31299. Drs. R. D. Veenstra and E. C. Beyer are Established Investigators of the American Heart Association.

REFERENCES

Beyer, E. C. 1990. Molecular cloning and developmental expression of two chick embryo gap junction proteins. *J. Biol. Chem.* 265:14439–14443.

Beyer, E. C., D. L. Paul, and D. A. Goodenough. 1990. Connexin family of gap junction proteins. *J. Membr. Biol.* 116:187–194.

Brink, P. R., and M. M. Dewey. 1980. Evidence for fixed charge in the nexus. *Nature.* 285:101–102.

Brink, P. R., and S.-F. Fan. 1989. Patch clamp recordings from membranes which contain gap junction channels. *Biophys. J.* 56:579–593.

Bukauskas, F., C. Kempf, and R. Weingart. 1992. Electrical coupling between cells of the insect *Aedes albopictus*. *J. Physiol. (Lond.).* 448: 321–337.

Chen, Y., and R. L. DeHaan. 1992. Multiple-channel conductance states and voltage regulation of embryonic chick cardiac gap junctions. *J. Membr. Biol.* 127:95–111.

Chen, Y., and R. L. DeHaan. 1993. Temperature dependence of embryonic cardiac gap junction conductance and channel kinetics. *J. Membr. Biol.* 136:125–134.

Colquhoun, C., and A. G Hawkes. 1983. Principles of stochastic interpretation of ion-channel mechanisms. *In* Single Channel Recording. B. Sakmann and E. Neher, editors. Plenum Press, New York. 135–175.

Dunlap, K., K. Takeda, and P. Brehm. 1987. Activation of a calcium-dependent photoprotein by chemical signaling through gap junctions. *Nature.* 325:60–62.

Ebihara, L., E. C. Beyer, K. I. Swenson, D. L. Paul, and D. A. Goodenough. 1989. Cloning and expression of a *Xenopus* embryonic gap junction protein. *Science.* 243:1194–1195.

Eisenman, G. 1962. Cation selective glass electrodes and their mode of operation. *Biophys. J.* 2:259–323.

El-Fouly, M. H., J. E. Trosko, and C.-C Chang. 1987. Scrape-loading and dye transfer. A rapid and simple technique to study gap junctional intercellular communication. *Exp. Cell Res.* 168:422–430.

Fishman, G. I., A. P. Moreno, D. C. Spray, and L. A. Leinwand. 1991. Functional analysis of human cardiac gap junction channel mutants. *Proc. Natl. Acad. Sci. USA.* 88:3525–3529.

Fishman, G. I., D. C. Spray, and L. A Leinwand. 1990. Molecular characterization and functional expression of the human cardiac gap junction channel. *J. Cell Biol.* 111:589–598.

Flagg-Newton, J., G. Dahl, and W. R. Loewenstein. 1981. Cell junction and cyclic AMP. I. Upregulation of junctional membrane permeability and junctional membrane particles by administration of cyclic nucleotide or phosphodiesterase inhibitor. *J. Membr. Biol.* 63:105–121.

Flagg-Newton, J., I. Simpson, and W. R. Loewenstein. 1979. Permeability of the cell-to-cell membrane channels in mammalian cell junction. *Science.* 205:404–407.

Fox, A. J. 1987. Ion channel subconductance states. *J. Membr. Biol.* 97:1–8.

Fuhlbridge, R. C., S. M. Fine, E. R. Unanue, and D. D. Chaplin. 1988. Expression of membrane interleukin 1 by fibroblasts transfected with murine pro-interleukin 1α cDNA. *Proc. Natl. Acad. Sci. USA.* 85:5649–5653.

Hennemann, H., H.-J. Schwarz, and K. Willecke. 1992. Characterization of gap junction genes expressed in F9 embryonic carcinoma cells: molecular cloning of mouse connexin31 and -45 cDNAs. *Eur. J. Cell Biol.* 57:51–58.

Hille, B. 1992. Ionic Channels of Excitable Membranes. Sinauer Associates Inc., Sunderland, MA. 607 pp.

Imanaga, I., M. Kameyama, and H. Irisawa. 1987. Cell-to-cell diffusion of fluorescent dyes in paired ventricular cells. *Am. J. Physiol.* 252: H223–H232.

Imoto, K., C. Busch, B. Sakmann, M. Mishina, T. Konno, J. Nakai, H. Bujo, Y. Mori, K. Fukuda, and S. Numa. 1988. Rings of negatively charged amino acids determine the acetylcholine receptor channel conductance. *Nature.* 335:645–648.

Kanter, H. L., J. E. Saffitz, and E. C. Beyer. 1992. Cardiac myocytes express multiple gap junction proteins. *Circ. Res.* 70:438–444.

Karasiewicz, J. 1981. Electron microscopic studies of cytokinesis in metazoan cells. *In* Mitosis/Cytokinesis. A. M. Zimmerman and A. Forer, editors. Academic Press, New York. 419–436.

Kolb, H.-A., and R. Somogyi. 1991. Biochemical and biophysical analysis of cell-to-cell channels and regulation of gap junction permeability. *Rev. Physiol. Biochem. Pharmacol.* 118:1–47.

Makowski, L., D. L. D. Caspar, W. C. Phillips, and D. A. Goodenough. 1984. Gap junction structures. V. Structural chemistry inferred from X-ray diffraction measurements on sucrose accessibility and trypsin susceptibility. *J. Mol. Biol.* 174:449–481.

Manivannan, K., S. V. Ramanan, R. T. Mathias, and P. R. Brink. 1992. Multichannel recordings from membranes which contain gap junctions. *Biophys. J.* 61:216–227.

Mantz, J., J. Cordier, and C. Giaume. 1993. Effects of general anesthetics on intercellular communications mediated by gap junctions between astrocytes in primary culture. *Anesthesiology.* 78:892–901.

Moreno, A. P., B. Eghbali, and D. C. Spray. 1991a. Connexin32 gap junction channels in stably transfected cells. Unitary conductance. *Biophys. J.* 60:1254–1266.

Moreno, A. P., B. Eghbali, and D. C. Spray. 1991b. Connexin32 gap junction channels in stably transfected cells. Equilibrium and kinetic properties. *Biophys. J.* 60:1267–1277.

Moreno, A. P., G. I. Fishman, and D. C. Spray. 1992. Phosphorylation shifts unitary conductance and modifies voltage-dependent kinetics of human connexin43 gap junction channels. *Biophys. J.* 62:51–53.

Neyton, J., and A. Trautmann. 1985. Single-channel currents of an intercellular junction. *Nature.* 317:331–335.

Nicholson, B. J., R. Dermietzel, D. Teplow, O. Traub, K. Willecke, and J.-P. Revel. 1987. Hepatic gap junctions are comprised of two homologous proteins of M_r 28,000 and M_r 21,000. *Nature.* 329:732–734.

Ramanan, S. V., and, P. R. Brink. 1993. Multichannel recordings from membranes which contain gap junctions. II. Substates and conductance shifts. *Biophys. J.* 65:1387–1395.

Reed, K. E., E. M. Westphale, D. M. Larson, H.-Z. Wang, R. D. Veenstra, and E. C. Beyer. 1993. Molecular cloning and functional expression of human connexin37, an endothelial cell gap junction protein. *J. Clin. Invest.* 91:997–1004.

Rubin, J. B., V. K. Verselis, M. V. L. Bennett, and T. A. Bargiello. 1992. Molecular analysis of voltage dependence of heterotypic gap junctions formed by connexins 26 and 32. *Biophys. J.* 62:183–195.

Rup, D. M., R. D. Veenstra, H.-Z. Wang, P. R. Brink, and E. C. Beyer. 1993. Chick connexin-56, a novel lens gap junction protein. *J. Biol. Chem.* 268:706–712.

Saez, J. C., J. A. Connor, D. C. Spray, and M. V. L. Bennett. 1989. Hepatocyte gap junctions are permeable to the second messenger, inositol 1:4,5-trisphosphate, and to calcium ions. *Proc. Natl. Acad. Sci. USA.* 86:2708–2712.

Safranyos, R. G. A., S. Caveney, J. G. Miller, and N. O. Petersen. 1987. Relative roles of gap junction channels and cytoplasm in cell-to-cell diffusion of fluorescent tracers. *Proc. Natl. Acad. Sci. USA.* 84:2272–2276.

Schwarzmann, G., H. Wiegandt, B. Rose, A. Zimmerman, D. Ben-Haim, and W. R. Loewenstein. 1981. Diameter of cell-to-cell junctional membrane channels as probed with neutral molecules. *Science*. 213:551–553.

Simpson, I., B. Rose, and W. R. Loewenstein. 1977. Size limit of molecules permeating the junctional membrane channels. *Science*. 195:294–296.

Spray, D. C., and J. Burt. 1990. Structure-activity relations of the cardiac gap junction channel. *Am. J. Physiol.* 258:C195–C205.

Spray, D. C., L. Cherbas, P. Cherbas, E. A. Morales, and G. M. Coaarow. 1989. Ionic coupling and mitotic synchrony of siblings in a *Drosophila* cell line. *Exp. Cell Res.* 184:509–517.

Swenson, K. I., J. R. Jordan, E. C. Beyer, and D. L. Paul. 1989. Formation of gap junctions by expression of connexins in *Xenopus* oocyte pairs. *Cell*. 57:145–155.

Tsien, R. W., and R Weingart. 1976. Inotropic effect of cyclic AMP in calf ventricular muscle studied by a cut end method. *J. Physiol. (Lond.)*. 260: 117–141.

Veenstra, R. D. 1991. Developmental changes in regulation of embryonic chick heart gap junctions. *J. Membr. Biol.* 119:253–265.

Veenstra, R. D., and P. R. Brink 1992. Patch clamp analysis of gap junctional currents. *In* Cell-Cell Interactions: A Practical Approach. B. Stevenson, D. L. Paul, and W. Gallin, editors. IRL Press, Oxford, England. 167–201.

Veenstra, R. D., and R. L. DeHaan. 1986. Measurement of single channel currents from cardiac gap junctions. *Science*. 233:972–974.

Veenstra, R. D., H.-Z. Wang, E. C. Beyer, and P. R. Brink. 1993. Differential permeability of connexin-specific gap junctions to flourescent tracers. *Biophys. J.* 64:235*a*. (Abstr.)

Veenstra, R. D., H.-Z. Wang, E. M. Westphale, and E. C. Beyer. 1992. Multiple connexins confer distinct regulatory and conductance properties of gap junctions in developing heart. *Circ. Res.* 71:1277–1283.

Verselis, V., and P. R. Brink. 1986. The gap junction channel. Its aqueous nature as indicated by deuterium oxide effects. *Biophys. J.* 50: 1003–1008.

Werner, R., E. Levine, C. Rabadan-Diehl, and G. Dahl. 1989. Formation of hybrid cell-cell channels. *Proc. Natl. Acad. Sci. USA*. 86:5380–5384.